Atomic insights into hydrodesulfurization

Prabhu, M.K.

Chapter 4

Simultaneous sulfidation of Mo and Co oxides supported on Au(111)

This chapter is based on :

Prabhu, M. K.; Groot, I. M. N. Simultaneous sulfidation of Mo and Co oxides supported on Au(111), Phys. Chem. Chem. Phys. ***2021****,23, 8403-8412*

Abstract

In this chapter, we present the results of a study carried out to investigate the simultaneous sulfidation of Co and Mo oxide nanoparticles on Au(111) as a synthesis strategy to prepare a model catalyst for hydrodesulfurization (HDS). We make use of scanning tunneling microscopy and X-ray photoelectron spectroscopy to track the changes in chemistry and morphology through the synthesis of a mixed Mo and Co oxide precursor and the sulfidation to the respective sulfides. We investigated the effects of temperature and the duration of sulfidation on the completeness of the sulfidation process. Our study shows that the formation of MoS_2 with the CoMoS edge is not affected by the time or the temperature of sulfidation. However, the yield of the Co-promoted MoS_2 slabs is limited by the formation of large clusters due to the spreading of Mo and Co oxide phases upon sulfidation. Complete sulfidation of the mixed oxide precursor to Co-promoted MoS_2 can be accelerated by increasing the sulfidation temperature to 730 K due to the thermally activated nature of Mo oxide sulfidation. Thus, we demonstrate that using a mixed Mo and Co oxide precursor as a starting point for Co-promoted MoS_2 phase for fundamental catalysis studies is a viable strategy.

4.1 Introduction

Graphite-like layered materials such as the transition metal dichalcogenides (TMDC) have garnered a lot of attention from the scientific community over the last decade.[1] The atomic structure of TMDCs consists of a layer of metal atoms sandwiched between two layers of chalcogen(S, Se or Te) atoms resulting in an MX_2-type stoichiometry. In the bulk, such molecular layers are held together by van der Waals forces. Like graphene from graphite, single-layer (SL) TMDCs can be exfoliated from the bulk.[2] The most widely studied among SL TMDCs include MoS_2 and WS_2.[3] SL MoS_2 has a direct band gap unlike its bulk counterpart and has found applications in a variety of fields such as electronics[4], biochemistry[5], efficient energy harvesting and storage[6,7] and catalysis.[8]

In many of these applications, nanosheets of SL MoS_2 deposited on substrates like Au(111)[9,10], highly-oriented pyrolytic graphite[11] and TiO_2(110)[12–14] are employed. Typically, these nanosheets are doped with foreign metal atoms such as Co or Ni to enhance their properties, for instance, the catalytic activity. Such doped SL MoS_2 slabs have been widely used in catalytic applications such as hydrodesulfurization (HDS)[15,16], CO_2 hydrogenation[17] and in fuel cell electrodes.[18,19] The SL Co- or Ni-promoted MoS_2 for these applications is usually grown by wet chemical methods[16], chemical vapor deposition (CVD)[20], thermal decomposition[21] or physical vapor deposition (PVD).[22,23] PVD in particular is useful for producing high quality promoted SL MoS_2 slabs and thus, has been the choice method for synthesizing the Co-promoted MoS_2 for fundamental research. The PVD method makes use of a mixture of metallic Co and Mo nanoparticles as the precursor. The metal nanoparticles being highly reactive, readily form promoted MoS_2 slabs in the presence of a chalcogen containing reactive gas such as H_2S.[23] In many of the industrially relevant synthesis strategies such as the wet impregnation method, however, the precursor to form the promoted MoS_2 nanoparticles, for instance, Co-promoted MoS_2, is a mixture of the respective oxides: Mo oxide and Co oxide. As an example, the HDS catalyst containing Co-promoted MoS_2 can be formed by sulfiding a mixture of MoO_3 and Co_3O_4 nanoparticles.[24,25] The transformation of the metal oxide nanoparticles to metal sulfide can show more complex behavior than the respective metal nanoparticles because of the reducibility of the oxides and the metal oxidation state dependent susceptibility towards sulfidation.[26–28] From the point of view of real catalysts used in the industry, it is important to understand the process of sulfiding a mixture of Mo and Co oxide nanoparticles in order to control the morphology of the Co-promoted MoS_2 slabs.

Molybdenum oxides have been studied on supports such as Au(111)[28–32], highly-oriented pyrolytic graphite (HOPG)[33], NiAl[34] and TiO_2(110).[35] The typical preparation methods used in these studies involve direct sublimation of MoO_3 powder, oxidation of Mo clusters, or CVD-like processes involving carbonyl complexes of Mo with NO_2 as the oxidizing agent. Additionally, the prior work carried out in our group[34] demonstrates a method of directly depositing Mo oxides from a source containing Mo metal. Co oxide has been synthesized by oxidizing Co nanoclusters on substrates like Ag(111)[36], Pt(111)[37,38] and Au(111).[39–44] This method produces pristine Co oxide slabs containing Co^{2+} and Co^{3+} depending on the oxygen background pressure used; higher O_2 pressures resulting in higher oxidation state of the metal atom. The Co oxide slabs thus formed, are known to have layered Co-O or O-Co-O-type structures. The oxidation and the reduction of these slabs have also been observed.[36,42,43]

Recently, sulfidation of MoO_3 supported on Au(111) was studied using a scanning tunneling microscope (STM) and X-ray photoelectron spectroscopy (XPS).[28] It was shown that the progressive annealing of the PVD-grown MoO_3 results in the reduction of Mo^{6+} to lower oxidation states, thus forming sub-stoichiometric Mo oxides. This causes morphological changes in the nanoparticles. Extensive sulfidation with H_2S was found to be necessary to form SL MoS_2 slabs as the oxide phase readily undergoes reduction and oxygen-sulfur exchange to form a stable oxysulfide phase, thereby hindering the complete sulfidation. It was observed that the sulfidation to MoS_2 was most efficient when Mo remained predominantly in its highest oxidation state, namely, Mo^{6+}. The sulfidation of aforementioned cobalt oxide slabs on the other hand, have not been studied so far. The sulfidation to Co_9S_8 and Co_3S_4 have been observed in sorbents containing Co_3O_4 supported on TiO_2.[45] However, fundamental studies involving sulfidation of cobalt oxides have predominantly been performed in conjunction with Mo oxide nanoparticles as a method to synthesize catalysts for HDS.[21,46–48] Furthermore, extensive studies in the last decade have shown that STM is a very powerful technique for directly observing the incorporation of Co atoms in the MoS_2 phase.[22,23,49]

In this chapter, we aim to gain insights into the sulfidation of a mixture of Co and Mo oxide precursor. Particularly, we investigate the formation of the Co-promoted MoS_2 phase. In order to do this, we first synthesize a precursor containing nanoparticles of Mo and Co oxides on an Au(111) substrate. Thereafter, the mixed oxide precursor is sulfided using hydrogen sulfide at 650 K for 25 to 90 minutes and at 730 K for 25 minutes in order to investigate the effects of time and temperature on the completeness of the sulfidation process and the formation of the Co-promoted MoS_2 phase. Using a combination of STM and XPS, we observe the formation of large clusters containing the 2D CoS_2 and the Co-promoted MoS_2 phases as well as individual SL Co-promoted MoS_2 nanoclusters. The results presented in this study show that by using a mixed oxide precursor as a starting point, the Co-promoted MoS_2 phase can be synthesized, albeit with a low yield due to the kinetically-hindered sulfidation of Mo oxide.

4.2 Experimental Methods

4.2.1 Substrate cleaning

The experiments described in this Chapter were carried out in the ReactorSTM setup.[50] The Au(111) single crystal was purchased from Surface Preparation Laboratory and cleaned with cycles of sputtering and annealing. Sputter cleaning with Ar^+ was performed under an argon atmosphere of $1x10^{-6}$ mbar and with an ion energy of 1.5 keV. The Au(111) single crystal was then annealed to 850 K using radiative heating for 45 minutes to obtain atomically flat gold terraces. The cleanliness was checked with XPS and STM until impurities were below the detection limits.

4.2.2 Deposition of Co and Mo oxides

Deposition of the Mo and Co oxides was performed using an Oxford EGCO4 e-beam evaporator. In the case of Mo oxide, the Mo rod was heated to ~1100 K in an oxygen atmosphere of $1x10^{-5}$ mbar. At

this temperature the vapor pressure of metallic Mo is negligible. However, the Mo^{6+} oxide formed on the Mo rod sublimes and deposits onto the sample held at 300 K. By maintaining the O_2 background pressure low, formation of Mo^{6+} on the rod can be controlled and therefore we can suppress the sublimation of Mo oxide polymers and ensure that small nanoparticles of Mo oxide are formed. The sample was then annealed to 500 K for 20 minutes while maintaining the background oxygen pressure. A doser was used to increase the local O_2 pressure near the sample ($>10^{-4}$ mbar) to suppress the reduction of Mo oxides to lower oxidation states. Subsequently, the sample was cooled to 300 K under the same O_2-rich atmosphere.

Cobalt oxide was grown by depositing metallic cobalt at 300 K in an O_2 atmosphere of $1x10^{-6}$ mbar followed by annealing at 600 K for 30 minutes while maintaining the oxygen background. The sample was cooled to room temperature in the same oxygen atmosphere. This recipe has been adapted from literature and is known to grow layered cobalt oxides on Au(111).[36,44]

4.2.3 Sulfidation

Sulfidation of the mixed Mo and Co oxide samples was carried out in an H_2S atmosphere of $2.5x10^{-6}$ mbar. Separate identical samples were prepared for investigating the effects of sulfidation at 650 K for 25 to 90 minutes and at 730 K for 25 minutes. In this manner, we aim to gain insights into the effects of the duration and the temperature of sulfidation. All the samples were cooled after sulfidation to 473 K maintaining the H_2S background after which the sample was allowed to cool to 300 K in ultra-high vacuum (UHV).

4.2.4 Scanning tunneling microscopy

Scanning tunneling microscopy was performed at room temperature using the UHV mode of the ReactorSTM. Tips were prepared from polycrystalline Pt-Ir 90-10 wire purchased from Goodfellow without further processing. Constant current scans were performed using LPM video-rate scanning electronics described in detail elsewhere.[51,52] Image processing was performed with a combination of home-developed Camera software and WSxM.[53,54] Most common normal filtering was used to obtain a correctly connected surface in order to calculate the height profiles. No other further processing was performed on the images reported in this Chapter.

4.2.5 X-ray photoelectron spectroscopy (XPS)

The XPS measurements were performed in a SPECS Phoibos system equipped with an XRM50 X-ray source set to the Al K-alpha line used along with a monochromator to excite the sample with a beam spot of 0.4 mm diameter at 55^{o} incidence. The acceleration voltage was set to 10 kV and a power of 250 W was used for all the measurements. The HSA3500 hemispherical analyzer with a pass energy of 30 eV was used to analyze the photoemission. The Au 4f peak set to 84.0 eV was used to calibrate the XPS spectra obtained. The number of integrations was set to 20. The data thus obtained, were characterized and quantified using CASA-XPS and XPSPEAK41 software with relative sensitivity factors for surfaces.[55] Gaussian-Leorentzian (35) curves were used for peak fitting using a Newton-Raphson algorithm after applying a Shirley background subtraction. For Mo 3d spectra, doublets with

a spacing of 3.15 eV due to the spin-orbit splitting of the Mo 3d signal were used for peak fitting each of the components arising from Mo and while a singlet was used for the S 2s component. The parameters used for peak fitting are tabulated in Table 1. The peak positions of the components were obtained from previously reported literature work.[28,31,56–59]

Table 1: XPS peak fitting parameters of the Mo 3d and Co $2p_{3/2}$ spectra

Component for Co $2p_{3/2}$	**Peak position (eV)**	**Component for Mo 3d**	**Peak position (eV)**
Co^{2+} oxide	780	Mo^{6+} oxide	233.1*
Co^{2+} oxide satellite 1	782	Mo^{5+} oxide	231.5*
Co^{2+} oxide satellite 2	785.4	Mo^{4+} oxide	230.6*
Co^{2+} oxide satellite 3	786.4	Mo^{4+} sulfide	229.2*
Co^{3+} oxide	779.5	Mo metal	228.1*
Co^{3+} oxide satellite 1	780.8	S 2s	226
Co^{3+} oxide satellite 2	782.1		
Co^{3+} oxide satellite 3	785.1		
Co^{3+} oxide satellite 4	789.4		
Co metal	778.3		
Co metal satellite 1	781.3		
Co metal satellite 2	783.3		
CoS_2	778.1		
CoS_2 satellite 1	781.1		
CoS_2 satellite 2	783.1		

*Peak positions are of the $3d_{5/2}$ component

4.3 Results

In order to prepare a mixed Mo and Co oxide precursor, we start with the growth of Co oxide slabs on Au(111). After the deposition of ~0.05 monolayers (ML) Co in an O_2 atmosphere followed by oxidation of the Co nanoparticles at 600 K, the Au(111) surface is covered with slabs of cobalt oxide (see Figure 1a) which are 6-10 nm in size. The slabs are atomically flat and have a truncated hexagonal shape. Most of the slabs of cobalt oxide have a measured height of 4.1 Å (see Figure 1b) while some of them have a height of 1.9 Å. We observed that the later was formed mostly around the step edges of Au(111). Additionally, the Co oxide slabs have a diffuse hexagonal pattern (inset Figure 1a) on their basal plane. We identify this as a moiré structure due to lattice mismatch with the underlying Au(111) surface. The moiré structures of the cobalt oxide slabs which are 4.1 Å high have a rotation of ~6° with respect to that of the slabs which are 1.9 Å high (see supporting information, Figure S1). All these observations match nicely with those of Walton et al.[44] who have shown with combined STM experiments and DFT calculations that Co oxide slabs grow as a layered -Co-O structure on Au(111). According to their experiments, Co oxide slabs with -Co-O-Co-O structure have measured heights of 4 Å on gold, while single -Co-O layer slabs have 1.7 Å heights. They have, however, observed a higher

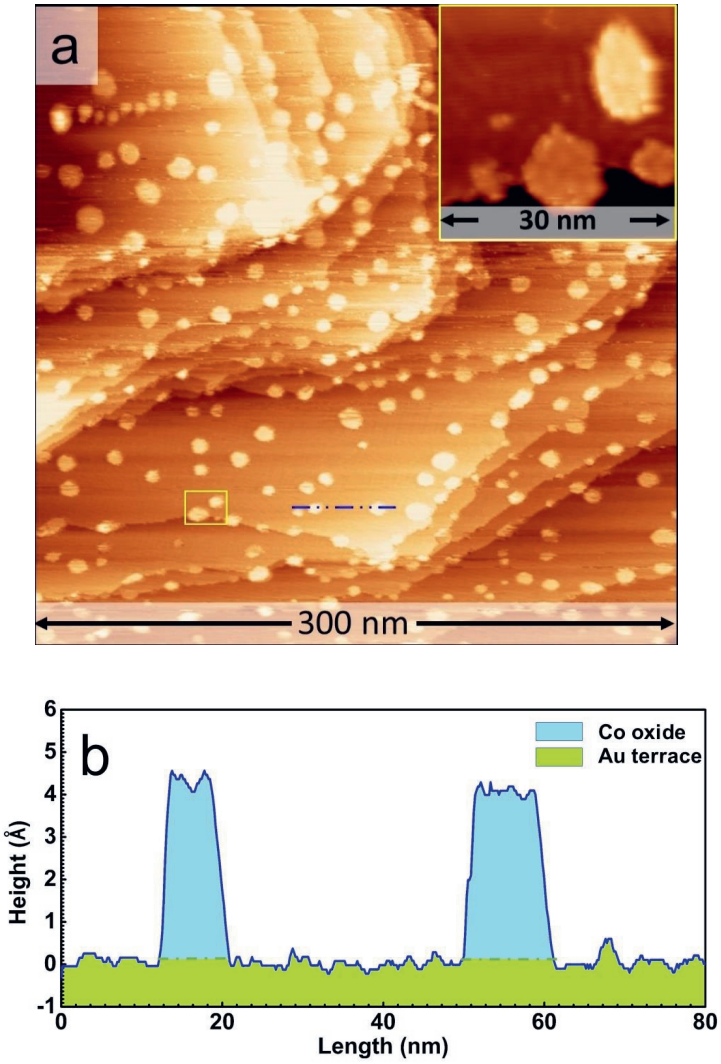

Figure 1:a) Large-scale STM image of Co oxide slabs on Au(111) obtained at sample voltage = -1.6 V, tunneling current = 150 pA. The inset shows the zoom-in of the region marked in yellow. The hexagonal moiré structure of the Co oxide slabs is clearly visible. b) Measured height along the blue dash-double dotted line in Figure 1a.

density of SL Co-O islands contrary to our experiment where the majority are 4.1 Å high. This disagreement could be due to the higher amount of Co deposited during synthesis in this study.

Mo oxide nanoparticles were grown on the sample containing Co oxide slabs supported on Au(111) by the direct deposition technique detailed in the experimental methods. Mo oxide was grown until ~0.05 ML Mo was detected on the sample using the XPS such that an Mo:Co ratio of ~1:1 could be achieved and Mo and Co together had a total coverage of ~10% of a monolayer on Au(111). This particular value was chosen because the typical techniques reported in literature for growing 2-3 nm slabs of Co-promoted MoS_2 involve the use of at most ~0.1 ML of metallic Co and Mo.[23] Our recipe resulted in the formation of Mo oxide nanoparticles with a 3D morphology (see Figure 2a). Most of the Mo oxide particles had a measured height of 9.5-11 Å (Figure 2b). Some Mo oxide nanoparticles were measured to have a height of 5.5-6 Å. The growth mode and the morphologies of Mo oxides deposited on Au(111) depends on the type of precursor used, the temperature of oxidation and the oxidizing agent.[30–32] Therefore, comparing the Mo oxide morphologies from our STM images with those from other Mo oxide synthesis methods on Au(111) reported in literature becomes difficult. To investigate the effects of Co oxide slabs on the Mo oxide morphology, we deposited Mo oxide nanoparticles directly on a clean Au(111) (see supporting information, Figure S2) in a separate experiment. We observed that the Mo oxide nanoparticles grown on clean Au(111) also have identical morphologies and measured STM heights, suggesting that the Mo oxide morphology is largely unaffected by the presence of Co oxide slabs on Au(111). However, we cannot rule out the possibility of some Mo oxide nanoparticles nucleating over a cobalt oxide slab. The Co oxide slabs, on the other hand, were observed to undergo changes in their morphology all of which can be attributed to the exposure to higher oxygen pressures ($>1\text{x}10^{-5}$ mbar) during the Mo oxide synthesis. The Co oxide slabs largely retained the truncated hexagonal shape but were observed to grow in height. We observed the presence of Co oxide slabs of 3 Å, 4 Å and 5 Å heights post-annealing (see supporting information, Figure S3). The previously grown SL Co oxide slabs of 2 Å height were not observed anymore after the synthesis of Mo oxides. Fester et al.[43] have observed that –Co-O- type Co oxide slabs exposed to higher oxygen pressures undergo systematic oxidation from Co^{2+} to Co^{3+} which results in the formation of -O-Co-O type slabs with measured height of 2.9 Å in their experiment. We propose that the Co oxide slabs measured with heights of 3 Å and 5 Å are single and multilayer stacks (O-Co-O-Co-O) respectively, each containing Co^{3+}, while those slabs with heights of 4 Å are likely the unconverted double Co-O layer slabs with Co^{2+}. It is also possible that some of the multilayer slabs consist of both Co^{2+} and Co^{3+} layers leading to an overall mixed oxidation state of Co.

The mixed Co and Mo oxide sample thus prepared, was chosen as the precursor for sulfidation using H_2S ($1\text{x}10^{-6}$ mbar). Figure 3a shows the large-scale STM image after the sulfidation at 650 K for 25 minutes. We observed the formation of two types of structures on the Au(111) surface post-sulfidation: a) large clusters of ~50 nm size, b) small hexagonal slabs. The large clusters consist of three phases (see Figure 3a) with the outer two phases marked 1 and 2 in Figure 3a being atomically flat while the inner phase marked 3 being atomically rough. Phase 1 and 2 were often observed to encapsulate the phase 3 as seen in Figure 3a. The small hexagonal slabs are discussed later in this chapter.

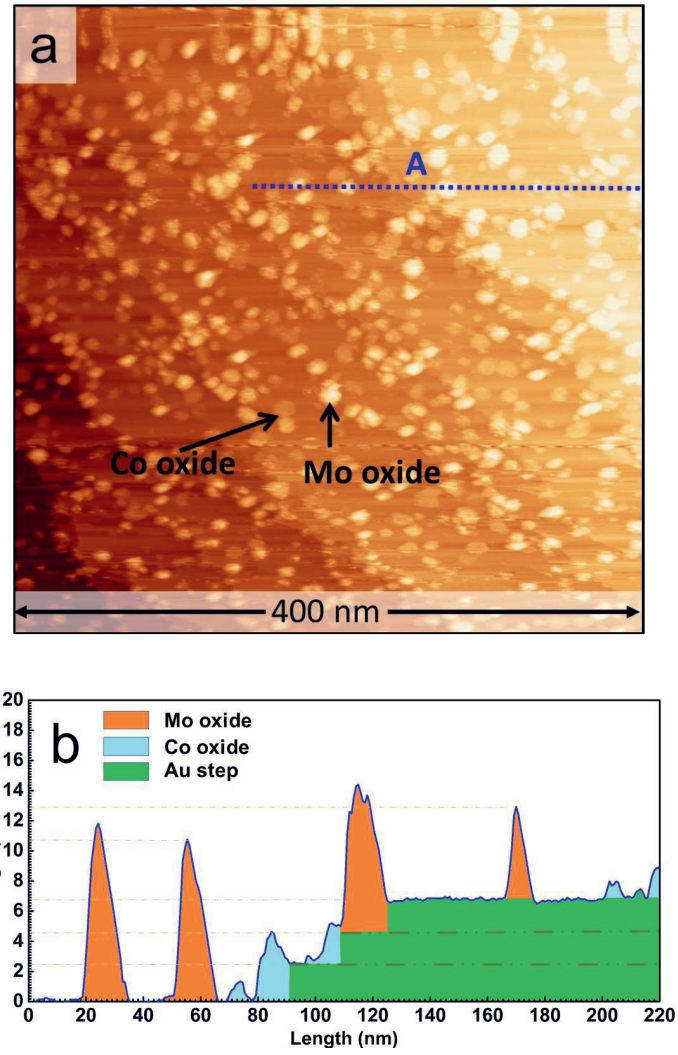

Figure 2: a) Large-scale STM image of Mo oxide nanoparticles deposited on the Au(111) sample containing Co oxide slabs, sample voltage = -1.5 V, tunneling current = 150 pA. b) Measured height along the blue dashed line marked A in Figure 2a.

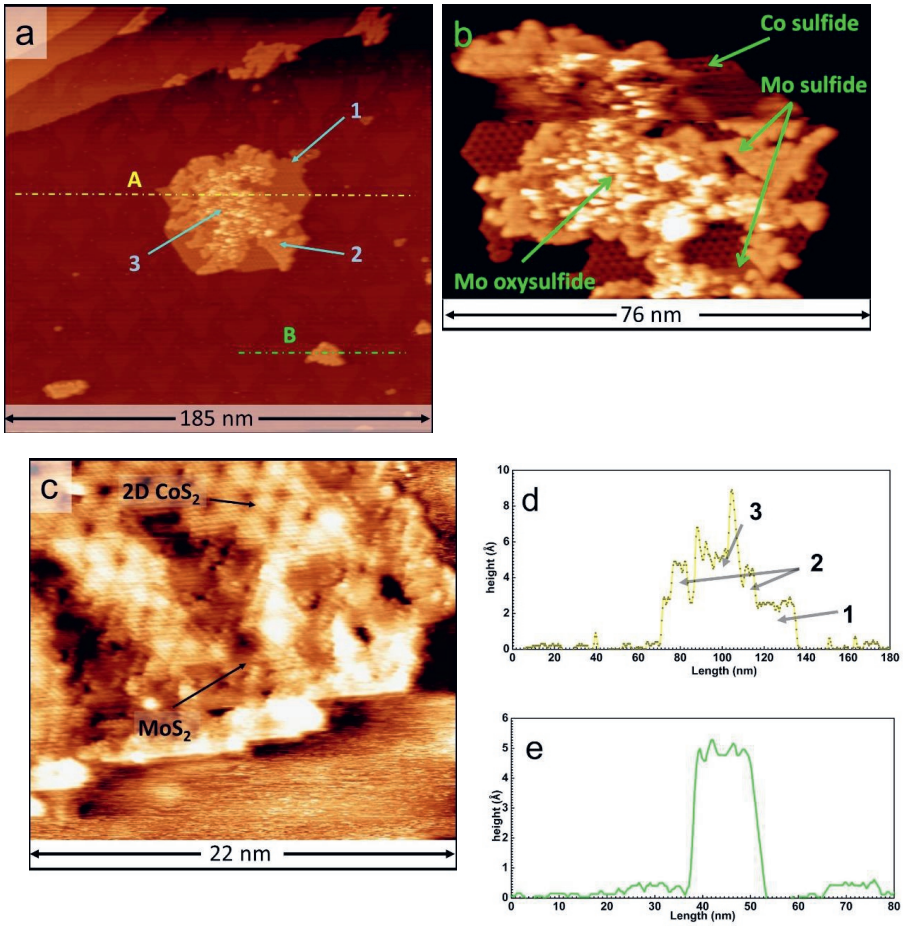

Figure 3:a) Large-scale STM image of the simultaneously sulfided Co and Mo oxides on the Au(111) substrate. Phase 1,2 and 3 are marked in the Figure; b) zoom-in of a large cluster containing the three phase. The MoS_2, 2D CoS_2, and partially sulfided Mo oxide phases are marked; c) Atom-resolved STM image of the defective MoS_2 phase in one of the large clusters; d, e) Measured height along the blue dashed lines marked A and B respectively in Figure 3a. The respective layers in Figure 3a and 3c have been marked as 1) 2D CoS_2 2) MoS_2 slabs 3) Partially sulfided Mo oxide. All of STM images in Figure 3 were acquired at sample voltage = -1.2 V and tunneling current = 200 pA.

Phase 1 has a low contrast in the STM image and has a hexagonal superstructure on its basal plane (see Figure 3b and 3c). This phase has a measured height of 2.4±0.2 Å (Figure 3d). We identify this phase as a SL 2D-CoS_2 sheet with an S-Co-S layered structure and the hexagonal super structure being a moiré pattern due to lattice mismatch with Au(111). The detailed structural characterization of this phase has been carried out in Chapter 3 and elsewhere in the literature.[60] Phase 2 has an intermediate contrast in the STM image in comparison to Phase 1 and 3. Additionally, its basal plane shows irregular contrast variations. We identify this layer as an MoS_2 slab which is not fully crystalline. These contrasts variations are attributed to the presence of a large number of defects which are resolved further in the atom-resolved STM image in Figure 3c. SL MoS_2 slabs on gold are reported to have a measured height of 2±0.3 Å.[9] However, we measure a height of 4.5±0.2 Å for the MoS_2 slabs present in phase 2 (see Figure 3d and 3e) suggesting the presence of a double layer. It is also possible that the second MoS_2 layer is supported over a layer of 2D CoS_2 sheet. The innermost phase marked 3, which has atomic roughness, is very likely an Mo oxysulfide phase. Reducible oxides of metals such as Mo, Ti and Ce are known to readily undergo O-S exchange even in vacuum pressures of H_2S.[28,61] Therefore, it is unlikely that any of the pure Mo oxides survive the annealing step in the presence of H_2S. Furthermore, prior experiments involving the sulfidation of Mo oxides supported on gold have shown that an intermediate oxysulfide phase can form during the sulfidation of the Mo oxide phase.[28]

Thus, the sulfidation carried out at 650 K for 25 minutes resulted in a partial conversion of the oxide phase and the formation of defective MoS_2 slabs. We devised two strategies to enhance the yield of the Mo and Co sulfide phase. For this, identical precursors of mixed Mo and Co oxide nanoparticles as in Figure 2a were prepared. In the first strategy, we increased the time of sulfidation systematically to up to 90 minutes. In the second, we increased the sulfidation temperature to 730 K while maintaining the time of sulfidation to 25 minutes. XPS was used to check for the completeness of the sulfidation process and STM images were acquired thereafter.

Figure 4a and 4b show the Co $2p_{3/2}$ and Mo 3d XPS spectra respectively, which were acquired for the samples after the initial synthesis of Co oxide slabs supported on Au(111), deposition of Mo oxide on the sample containing Co oxide supported on Au(111), and after 25 minutes of sulfidation at 650 K, 50 minutes of sulfidation at 650 K, 90 minutes of sulfidation at 650 K, and 25 minutes of sulfidation at 730 K. The Co $2p_{3/2}$ spectrum (Figure 4a) of the initially grown Co oxide slabs on Au(111) consists of contributions of a high-spin Co oxide and a Co metal component. The Co oxide component shows a broad main peak at 780 eV with a shoulder at 782 and 785.4 eV. Furthermore, a broad satellite feature at 786.4 eV is also detected. These observations are in agreement with prior experimental reports of –Co-O- type Co oxide slabs supported on Au(111)[42] and in line with our interpretation of the STM image in Figure 1a. The presence of Co metal component indicates that there is very likely Co that is alloyed with gold and is present in the sub-surface region as we do not observe any metallic Co phase in the STM images. After the deposition of Mo oxide, the main peak of the Co $2p_{3/2}$ spectrum shows a 0.6 eV shift towards higher binding energy at 780.6 eV (see Figure 4a). Peak fitting shows contributions from Co^{3+} oxide, Co^{2+} oxide as well as a minor contribution from Co metal. Figure 4a shows that the contribution from the Co^{2+} oxide and the Co metal component decreases significantly while the Co^{3+} component is dominant which suggests an oxidation of some of the Co^{2+} to Co^{3+}. This supports our observations from the STM images in Figure 2a which suggest a partial oxidation of the Co^{2+} slabs into slabs containing Co^{3+} oxide. Similar observations were also reported in the work of

Fester et al..[42,43] We note that the presence of CoOOH in the Co oxide slabs cannot be ruled out as its reference spectrum also has similar features to those of Co^{3+} oxide.[56] We, however, did not consider this component in our peak fitting. The Mo 3d spectrum of the Mo oxide deposited on the sample containing Co oxide slabs supported on Au(111) shows the presence of predominantly Mo^{6+} and Mo^{5+} oxidation states.[24,28] The higher local pressure of oxygen attained with the usage of a doser ensures that extensive thermal reduction of Mo oxides as in the work of Salazar et al.[28] is greatly suppressed.

Upon sulfidation, for all the conditions used, the Co $2p_{3/2}$ main peak shifts to lower binding energy at 778.1 eV, indicating a conversion to the sulfide. The satellite feature also shifts to 783.1 eV and is consistent with the reference spectra of 2D CoS_2 on Au(111)[60] and other supports.[24] Components from the Co^{2+} and Co^{3+} oxide were not observed for all the sulfided samples. This suggests that the sulfidation is complete within the first 25 minutes at 650 K itself. This is also in agreement with our observation of a pristine 2D CoS_2 phase in the STM images (phase 1, Figure 3a). The Mo 3d spectrum, on the other hand, shows a progressive shift to the Mo^{4+} oxidation state with increasing sulfidation time. Additionally a component at 226 eV of the S 2s signal is also detected. The Mo^{4+} and the S 2s features are attributed to the formation of MoS_2. The S 2s also likely has some contribution from sulfur adsorbed on Au(111) due to H_2S exposure. Furthermore, it is also possible that some of the Mo^{4+} component arises due to incomplete sulfidation and reduction of Mo oxide in the presence of H_2S. Some contributions from the Mo^{5+} and Mo^{6+} components are also detected. These components are attributed to Mo oxide phases that are not completely sulfided (phase 3, Figure 3a) and likely are present as an oxysulfide. After 90 minutes of sulfidation, the Mo 3d spectrum shows only the Mo^{4+} component characteristic of pristine MoS_2 [28] indicating complete sulfidation of Mo. However, traces of the incompletely sulfide phase were observed in the STM images obtained after 90 minutes of sulfidation at 650 K (see supporting information, Figure S4). After sulfidation at 730 K for 25 minutes, the Mo 3d spectrum shows only the Mo^{4+} and S 2s features characteristic of MoS_2 suggesting a complete conversion to MoS_2. For the corresponding O 1s and S 2p spectra, we refer to the supporting information, Figure S5.

Table 2: Ratio and coverage of Co and Mo determined from the XPS spectra in Figure 4

	Co: Mo	**Co coverage (ML)***	**Mo coverage (ML)***
Co oxide / Au(111)		0.061	
Mo oxide + Co oxide	0.98	0.055	0.056
sulfidation 650 k 25 min	1.05	0.061	0.058
sulfidation 650 k 50 min	1.02	0.062	0.061
sulfidation 650 k 90 min	1.04	0.059	0.057
sulfidation 730 k 25 min	0.83	0.042	0.050

*with respect to Au(111), ML = monolayers

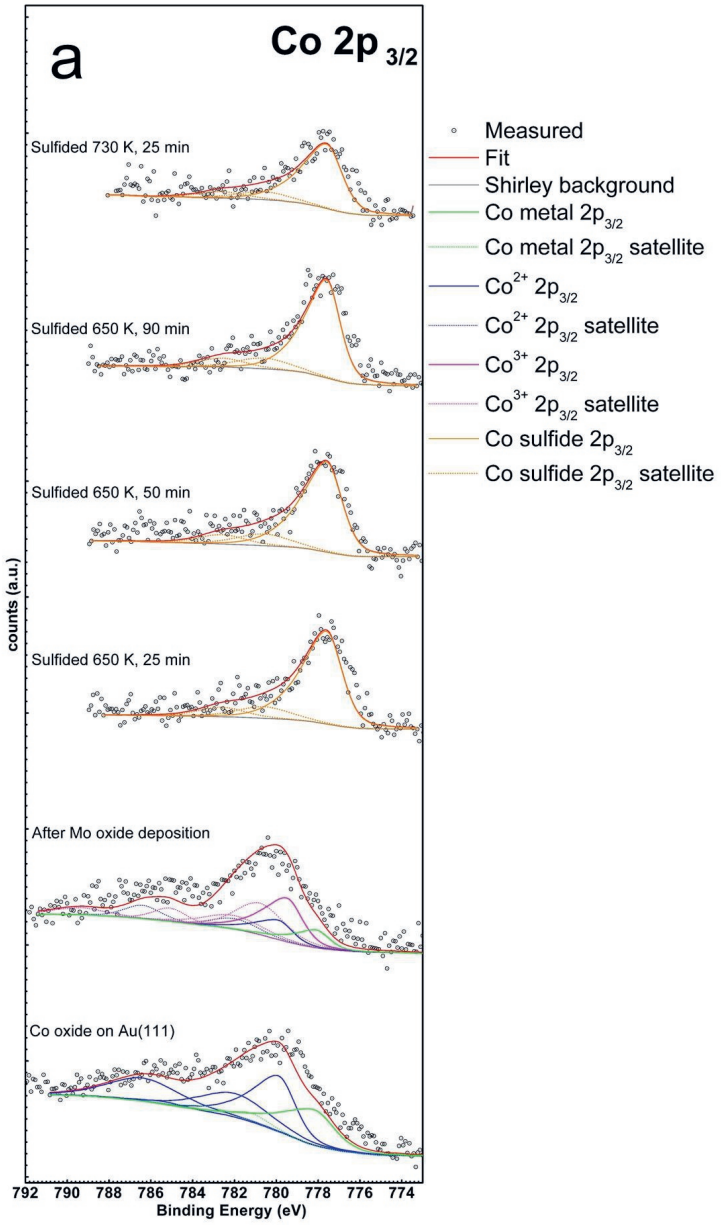
a
Co 2p 3/2
Sulfided 730 K, 25 min
Sulfided 650 K, 90 min
Sulfided 650 K, 50 min
Sulfided 650 K, 25 min
After Mo oxide deposition
Co oxide on Au(111)
counts (a.u.)
792 790 788 786 784 782 780 778 776 774
Binding Energy (eV)
Measured
Fit
Shirley background
Co metal 2p3/2
Co metal 2p3/2 satellite
Co2+ 2p3/2
Co2+ 2p3/2 satellite
Co3+ 2p3/2
Co3+ 2p3/2 satellite
Co sulfide 2p3/2
Co sulfide 2p3/2 satellite

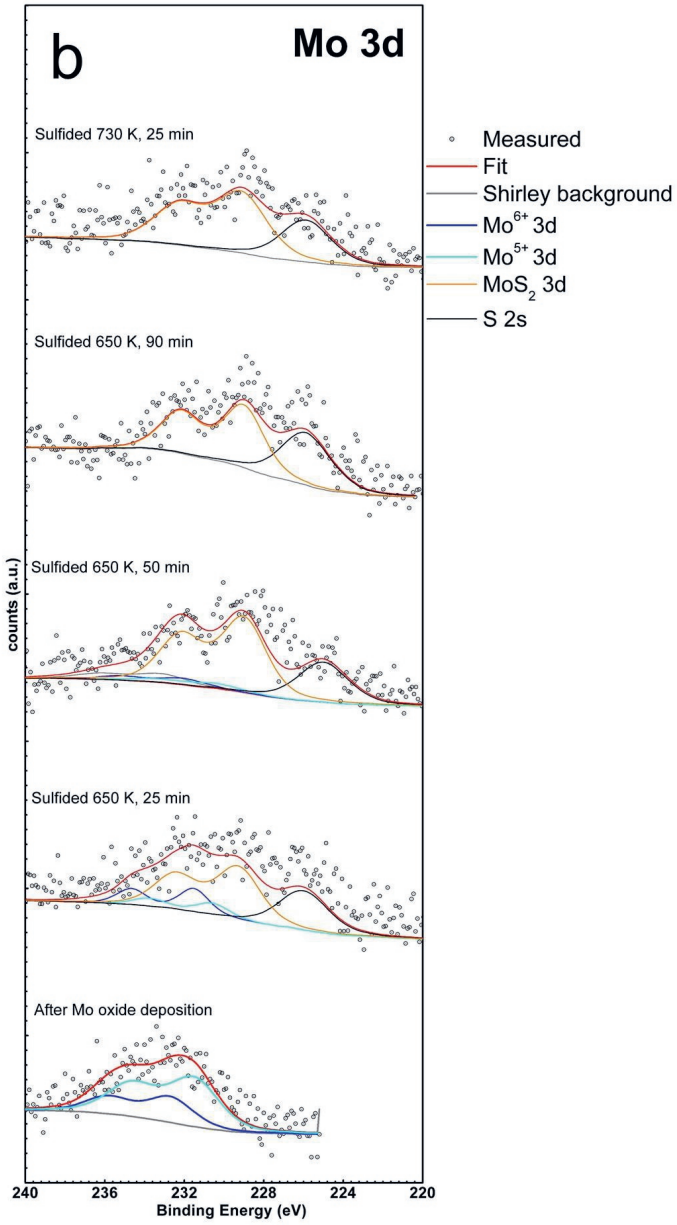

Figure 4: a,b) XPS spectra of Co $2p_{3/2}$ and Mo 3d regions respectively at various stages of oxide precursor synthesis and subsequent sulfidation.

We note that because of our ultimate aim of synthesizing small nanoclusters of the Co-promoted MoS_2 phase for catalytic studies, low coverages of Mo and Co are used in the experiments presented in this study. Therefore, it is only expected that the signal-to-noise ratio in the XPS data is low because of which there is greater uncertainty in the peak fitting used. However, due to the significant morphological changes occurring during the sulfidation process, it is important to obtain chemical information of our samples to gain more insights. Given the chemically blind nature of the STM and its inability to quantitatively probe the sub-surface, information on the coverages of Co and Mo obtained from the XPS is still very useful due to its ability to simultaneously probe the surface and the sub-surface atomic layers. The Co:Mo ratio and the coverages of the Co and Mo were estimated from the XPS spectra by taking into account the relative sensitivity factors of Co and Mo (see Table 2). The oxidic precursor containing the Co oxide slabs has a measured Co coverage of 0.061 ML. After the deposition of Mo oxide nanoparticles to 0.056 ML, the coverage of Co decreases to 0.055 ML. We attribute this decrease to a slight attenuation of the XPS signal of Co due to the Mo oxide growing over some of the Co oxide slabs. After sulfidation for 25 minutes at 650 K, we observe that the Co coverage is restored to the initial value of 0.061 ML while the Mo coverage only increases marginally resulting in a Co:Mo ratio of 1.05:1. This is a direct consequence of the morphological changes observed in the STM wherein both the Co and Mo oxides sulfide and spread on the surface to form large 2D clusters. The Co:Mo ratio as well as the coverages of Mo and Co remain constant with increasing time of sulfidation within the limits of the minute differences between the initial precursors prepared for each of the sulfidation experiments and the inherent uncertainty due to the lower signal-to-noise ratio in the XPS data. After sulfidation at 730 K for 25 minutes, however, we observe a significant decrease in the Co:Mo ratio as well as a decrease in the coverages of Co and Mo. We attribute this change to the increased tendency of Co and Mo oxides to reduce and alloy with Au at 730 K due to the surface of Au(111) being more sulfur-deficient than at 650 K. This leads to a partial lifting of the herringbone reconstruction and the formation of vacancy islands on the Au surface (see SI, Figure S4b).

In all of the sulfided samples studied in this chapter, individual SL slabs with a truncated hexagonal shape were also observed to form(Figure 5a). We identify these slab as the Co-promoted MoS_2 slabs. It is also known that MoS_2 slabs without the Co-promoter atoms adopt a fully triangular shape under sulfur-rich conditions that are used in this study. This is because the Mo-terminated edge is thermodynamically more favorable than the S-terminated edge for a pristine MoS_2 slab under S-rich conditions.[49] Incorporation of Co atoms into the S edge leads to thermodynamic stability and hence, the Co-promoted MoS_2 slabs adopt a hexagonal or truncated hexagonal shape displaying both the Mo- and S-terminated edges (see SI, Figure S6). Thus, the formation of hexagonal slabs under the sulfiding conditions used in our study is a signature of Co being incorporated into the S edges of the MoS_2 slabs.[49] Figure 5b shows the zoom in of a Co-promoted MoS_2 slab. It is known from prior STM experiments on MoS_2 that it is the sulfur atoms that are imaged as bright protrusions in the basal plane.[9] In Figure 5b, we observe that the penultimate row of protrusions along the edges of the Co-promoted MoS_2 slabs appear brighter than those in the basal plane. This feature is attributed to the electronic effects due to the 1D metallic edge states called as Brim sites.[9,49] In the past, a combination of STM experiments and DFT calculations has been used to show that the registry of the ultimate row of protrusions along the edges of a Co-promoted MoS_2 slabs with respect to the basal plane can be used to identify the type and the sulfur saturation of the edges.[49] In Figure 5b, the rows of atoms in the basal plane have been marked with green lines as a guide for the eyes. We observe that along

one of the edges, the bright protrusions are in registry with the basal plane protrusions. This is the signature of a 100% sulfur-saturated Co-substituted S edge.[49] On the adjacent edge, however, the edge protrusions are clearly out of registry with respect to the line of protrusions in the basal plane. This edge is identified as the 100% sulfur-saturated Mo-terminated edge in agreement with the work of Grønborg et al..[49] Figure 5c shows an atom-resolved STM image of a large cluster containing the MoS_2 and the 2D CoS_2 phase, measured after sulfidation for 90 minutes at 650 K. Based on the same method of edge identification, we identify the presence of Co-substituted S edge and the Mo-terminated edge in the MoS_2 phase (phase 2, Figure 3a) as well. This observation shows that the Co-substituted S edge is formed not only in the hexagonal SL Co-promoted MoS_2 slabs, but also in the MoS_2 phase present in the larger clusters as well.

4.4 Discussion

We have studied the process of growing a mixed Mo and Co oxide precursor and the subsequent transformation to Mo and Co sulfide through sulfidation with H_2S. We have carried out the sulfidation at 650 K for 25 to up to 90 minutes and at 730 K for 25 minutes. Our objective has been to gain insights into the process of oxide to sulfide conversion to form the Co-promoted MoS_2 phase.

Our results from XPS and STM show that there is a strong preference for the sulfidation of Co oxide. This is evident from the complete conversion of the Co oxide within the first 25 minutes of sulfidation. The sulfidation of Mo oxide on the other hand, is observed to be thermally activated. The sulfidation process is accompanied by a change in morphology from well-distributed nanoparticles and slabs to large clusters containing multiple phases. The formation of large clusters after the sulfidation process from a precursor containing oxide nanoparticles of Co and Mo can be driven by two factors, namely, the temperature and the presence of sulfur species. Annealing the oxidic precursor containing the Mo and Co oxides to 600 K in the absence of H_2S causes clustering of the Mo oxide phases (see SI, Figure S7). This clustering is accompanied by reduction of the Mo oxide phase as can be seen in the Mo 3d spectra in SI. Mo^{6+} oxide is known to undergo reduction to Mo^{5+} and Mo^{4+} states at temperatures above 600 K even in mild oxygen backgrounds ($\leq 1x10^{-6}$ mbar).[28,31,59] This thermal reduction is typically accompanied by a tendency to form large atomically flat clusters due to the underlying thermally activated cluster diffusion process.[29,31,59] The cobalt oxide slabs, on the other hand, are observed to be stable such heat treatments up to 650 K. However, in the presence of sulfur, diffusion of Co is known to be greatly enhanced due to the formation of Co-sulfur complexes even at 300 K.[62] Therefore, the observed morphological changes are very well in agreement with previous experimental reports.

Our STM experiments also show that the formation of the SL Co-promoted MoS_2 slabs with truncated hexagonal shape is not affected by the temperature or the duration of sulfidation as they are observed to form in all the sulfide samples studied in this chapter. Additionally, formation of the MoS_2 phase in the large clusters with the Co-substituted S edge is not hindered by the slower sulfidation of Mo oxide. However, the yield of individual SL Co-promoted MoS_2 slabs is significantly less than what would be obtained if the respective metallic precursors were used as a starting point such as in the recipes reported in literature.[23] This is mainly due to the tendency of the mixed oxide precursor to spread and form large clusters in the presence of sulfur and at elevated temperature, which then leads to differential sulfidation of the Co and Mo oxide phases in the cluster, thereby, reducing the yield of

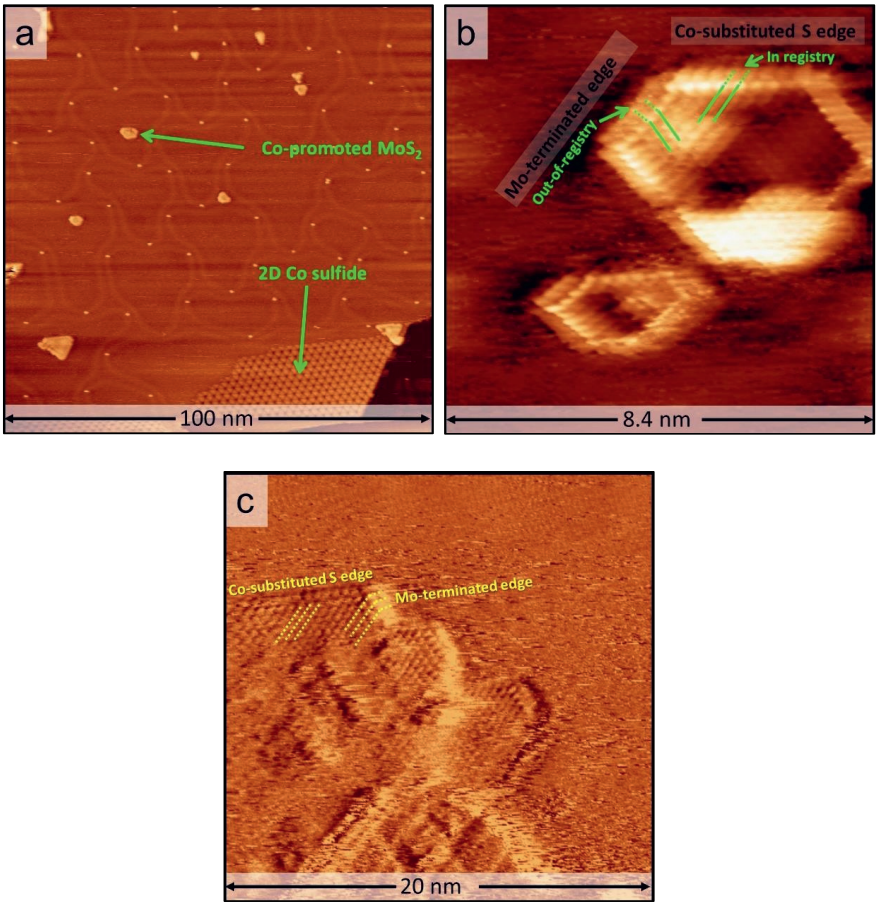

Figure 5:a) Large-scale STM image showing hexagonal MoS_2 slabs formed because of Co incorporation into the S edge, sample voltage = -1 V, tunneling current = 150 pA; b) Atom-resolved STM image of hexagonal Co-promoted MoS_2 slabs showing the Mo-terminated and the Co-substituted S edges, sample voltage = -0.5 V, tunneling current = 200 pA; ;c) Atom-resolved STM image of the MoS_2 slabs in the large clusters (phase 2), sample voltage = -0.35 V, tunneling current = 900 pA.

the Co-promoted MoS_2 phase. The Mo oxide phase that is not fully sulfided, is encapsulated by the 2D CoS_2 and the MoS_2 slabs as can be seen in the STM images presented in this chapter. This could create additional barriers for the sulfur atoms to diffuse into the partially converted Mo oxide phase. This is quite in contrast to the previously reported synthesis strategies that involve Au(111)-supported metallic Co and Mo nanoparticles as the precursor wherein, the nanoparticles readily sulfide and form Co-promoted MoS_2 slabs due to the absence of the oxysulfide phase.[23,49] Despite the low yield, we show that using a precursor with mixed Mo and Co oxides is a viable strategy to synthesize the Co-promoted MoS_2 phase in order to carry out fundamental studies relevant for fields such as catalysis. One possible strategy to increase the yield of individual Co-promoted MoS_2 slabs could involve starting with a precursor containing other ratios Mo and Co. Another solution may lay in the use of model supports like TiO_2(110) that interact strongly with Co and Mo oxides, and thus, prevent large clusters from forming.

4.5 Conclusions

Starting with a mixture of Mo and Co oxide nanoparticles on Au(111), we have investigated the process of their sulfidation using STM and XPS. We have shown that it is possible to synthesis SL Co-promoted MoS_2 slabs using this mixed oxide precursor independent of the temperature and duration of the sulfidation process. We have also shown that due to the tendency to reduce and spread on the surface, the Mo and Co oxides form large clusters that contain the MoS_2, 2D CoS_2 and likely an incompletely sulfided Mo oxide phase depending on the temperature and duration of the sulfidation. The MoS_2 slabs in these large clusters also have Co atoms incorporated in their S edges. Thus, we have shown that sulfiding a mixture of Co and Mo oxide nanoparticles is a feasible strategy to synthesize Co-promoted MoS_2 for fundamental catalysis studies, especially those for hydrodesulfurization.

.

4.6 References

(1) Liu, B.; Abbas, A.; Zhou, C. Two-Dimensional Semiconductors: From Materials Preparation to Electronic Applications. *Advanced Electronic Materials*. 2017, p 1700045. https://doi.org/10.1002/aelm.201700045.

(2) Bissett, M. A.; Worrall, S. D.; Kinloch, I. A.; Dryfe, R. A. W. Comparison of Two-Dimensional Transition Metal Dichalcogenides for Electrochemical Supercapacitors. *Electrochim. Acta* 2016, *201*, 30–37. https://doi.org/10.1016/j.electacta.2016.03.190.

(3) Manzeli, S.; Ovchinnikov, D.; Pasquier, D.; Yazyev, O. V.; Kis, A. 2D Transition Metal Dichalcogenides. *Nature Reviews Materials*. 2017, p 17033. https://doi.org/10.1038/natrevmats.2017.33.

(4) Lembke, D.; Bertolazzi, S.; Kis, A. Single-Layer MoS_2 Electronics. *Acc. Chem. Res.* 2015, *48* (1), 100–110. https://doi.org/10.1021/ar500274q.

(5) Yin, W.; Yan, L.; Yu, J.; Tian, G.; Zhou, L.; Zheng, X.; Zhang, X.; Yong, Y.; Li, J.; Gu, Z.; Zhao, Y. High-Throughput Synthesis of Single-Layer MoS_2 Nanosheets as a near-Infrared Photothermal-Triggered Drug Delivery for Effective Cancer Therapy. *ACS Nano* 2014, *8* (7), 6922–6933. https://doi.org/10.1021/nn501647j.

(6) Feng, J.; Graf, M.; Liu, K.; Ovchinnikov, D.; Dumcenco, D.; Heiranian, M.; Nandigana, V.; Aluru, N. R.; Kis, A.; Radenovic, A. Single-Layer MoS_2 Nanopores as Nanopower Generators. *Nature* 2016, *536* (7615), 197–200. https://doi.org/10.1038/nature18593.

(7) Wu, W.; Wang, L.; Li, Y.; Zhang, F.; Lin, L.; Niu, S.; Chenet, D.; Zhang, X.; Hao, Y.; Heinz, T. F.; Hone, J.; Wang, Z. L. Piezoelectricity of Single-Atomic-Layer MoS_2 for Energy Conversion and Piezotronics. *Nature* 2014, *514* (7253), 470–474. https://doi.org/10.1038/nature13792.

(8) Li, Y.; Li, Y. L.; Araujo, C. M.; Luo, W.; Ahuja, R. Single-Layer MoS_2 as an Efficient Photocatalyst. *Catal. Sci. Technol.* 2013, *3* (9), 2214–2220. https://doi.org/10.1039/c3cy00207a.

(9) Helveg, S.; Lauritsen, J. V.; Lægsgaard, E.; Stensgaard, I.; Nørskov, J. K.; Clausen, B. S.; Topsøe, H.; Besenbacher, F. Atomic-Scale Structure of Single-Layer MoS_2 Nanoclusters. *Phys. Rev. Lett.* 2000, *84* (5), 951–954. https://doi.org/10.1103/PhysRevLett.84.951.

(10) Grønborg, S. S.; Ulstrup, S.; Bianchi, M.; Dendzik, M.; Sanders, C. E.; Lauritsen, J. V.; Hofmann, P.; Miwa, J. A. Synthesis of Epitaxial Single-Layer MoS_2 on Au(111). *Langmuir* 2015, *31* (35), 9700–9706. https://doi.org/10.1021/acs.langmuir.5b02533.

(11) Kibsgaard, J.; Lauritsen, J. V.; Lægsgaard, E.; Clausen, B. S.; Topsøe, H.; Besenbacher, F. Cluster-Support Interactions and Morphology of MoS_2 Nanoclusters in a Graphite-Supported Hydrotreating Model Catalyst. *J. Am. Chem. Soc.* 2006, *128* (42), 13950–13958. https://doi.org/10.1021/ja0651106.

(12) Liu, H.; Li, Y.; Xiang, M.; Zeng, H.; Shao, X. Single-Layered MoS2 Directly Grown on Rutile TiO_2(110) for Enhanced Interfacial Charge Transfer. *ACS Nano* 2019, *13* (5), 6083–6089. https://doi.org/10.1021/acsnano.9b02608.

(13) Galhenage, R. P.; Yan, H.; Rawal, T. B.; Le, D.; Brandt, A. J.; Maddumapatabandi, T. D.; Nguyen, N.; Rahman, T. S.; Chen, D. A. MoS_2 Nanoclusters Grown on TiO_2: Evidence for New Adsorption Sites at Edges and Sulfur Vacancies. *J. Phys. Chem. C* 2019, *123* (12), 7185–7201. https://doi.org/10.1021/acs.jpcc.9b00076.

(14) Kibsgaard, J.; Clausen, B. S.; Topsøe, H.; Lægsgaard, E.; Lauritsen, J. V.; Besenbacher, F. Scanning Tunneling Microscopy Studies of TiO_2-Supported Hydrotreating Catalysts: Anisotropic Particle Shapes by Edge-Specific MoS_2-Support Bonding. *J. Catal.* 2009, *263* (1), 98–103. https://doi.org/10.1016/j.jcat.2009.01.016.

(15) Topsøe, H.; Clausen, B. S.; Candia, R.; Wivel, C.; Mørup, S. In Situ Mössbauer Emission Spectroscopy Studies of Unsupported and Supported Sulfided CoMo Hydrodesulfurization Catalysts: Evidence for and Nature of a CoMoS Phase. *J. Catal.* 1981, *68* (2), 433–452. https://doi.org/10.1016/0021-9517(81)90114-7.

(16) Dai, X.; Du, K.; Li, Z.; Liu, M.; Ma, Y.; Sun, H.; Zhang, X.; Yang, Y. Co-Doped MoS_2 Nanosheets with the Dominant CoMoS Phase Coated on Carbon as an Excellent Electrocatalyst for Hydrogen Evolution. *ACS Appl. Mater. Interfaces* 2015, *7* (49), 27242–27253. https://doi.org/10.1021/acsami.5b08420.

(17) Nieskens, D. L. S.; Ferrari, D.; Liu, Y.; Kolonko, R. The Conversion of Carbon Dioxide and Hydrogen into Methanol and Higher Alcohols. *Catal. Commun.* 2011, *14* (1), 111–113. https://doi.org/10.1016/j.catcom.2011.07.020.

(18) Escalera-López, D.; Niu, Y.; Yin, J.; Cooke, K.; Rees, N. V.; Palmer, R. E. Enhancement of the Hydrogen Evolution Reaction from Ni-MoS_2 Hybrid Nanoclusters. *ACS Catal.* 2016, *6* (9), 6008–6017. https://doi.org/10.1021/acscatal.6b01274.

(19) Deng, J.; Li, H.; Xiao, J.; Tu, Y.; Deng, D.; Yang, H.; Tian, H.; Li, J.; Ren, P.; Bao, X. Triggering the Electrocatalytic Hydrogen Evolution Activity of the Inert Two-Dimensional MoS_2 Surface via Single-Atom Metal Doping. *Energy Environ. Sci.* 2015, *8* (5), 1594–1601. https://doi.org/10.1039/c5ee00751h.

(20) Okamoto, Y. A Novel Preparation-Characterization Technique of Hydrodesulfurization Catalysts for Cleaner Fuels. *Catal. Today* 2008, *132* (1–4), 9–17. https://doi.org/10.1016/j.cattod.2007.12.030.

(21) Menart, M. J.; Hensley, J. E.; Costelow, K. E. Thermal Decomposition of Bulk K-$CoMoS_x$ Mixed Alcohol Catalyst Precursors and Effects on Catalyst Morphology and Performance. *Appl. Catal. A Gen.* 2012, *437–438*, 36–43. https://doi.org/10.1016/j.apcata.2012.06.010.

(22) Byskov, L. S.; Nørskov, J. K.; Clausen, B. S.; Topsøe, H. Edge Termination of MoS_2 and CoMoS Catalyst Particles. *Catal. Letters* 2000, *64* (2–4), 95–99. https://doi.org/10.1023/a:1019063709813.

(23) Lauritsen, J. V.; Kibsgaard, J.; Olesen, G. H.; Moses, P. G.; Hinnemann, B.; Helveg, S.; Nørskov, J. K.; Clausen, B. S.; Topsøe, H.; Lægsgaard, E.; Besenbacher, F. Location and Coordination of Promoter Atoms in Co- and Ni-Promoted MoS_2-Based Hydrotreating Catalysts. *J. Catal.* 2007, *249* (2), 220–233. https://doi.org/10.1016/j.jcat.2007.04.013.

(24) Leliveld, R. G.; Van Dillen, A. J.; Geus, J. W.; Koningsberger, D. C. The Sulfidation of γ-Alumina and Titania Supported (Cobalt)Molybdenum Oxide Catalysts Monitored by EXAFS. *J. Catal.* 1997, *171* (1), 115–129. https://doi.org/10.1006/jcat.1997.1783.

(25) Qian, W.; Ishihara, A.; Aoyama, Y.; Kabe, T. Sulfidation of Nickel- and Cobalt-Promoted Molybdenum-Alumina Catalysts Using a Radioisotope 35S-Labeled H_2S Pulse Tracer Method. *Appl. Catal. A Gen.* 2000, *196* (1), 103–110. https://doi.org/10.1016/S0926-860X(99)00454-8.

(26) Kobayashi, M.; Flytzani-Stephanopoulos, M. Reduction and Sulfidation Kinetics of Cerium Oxide and Cu-Modified Cerium Oxide. *Ind. Eng. Chem. Res.* 2002, *41* (13), 3115–3123. https://doi.org/10.1021/ie010815w.

(27) Chen, C. J.; Chiang, R. K. Sulfidation of Rock-Salt-Type Transition Metal Oxide Nanoparticles as an Example of a Solid State Reaction in Colloidal Nanoparticles. *Dalt. Trans.* 2011, *40* (4), 880–885. https://doi.org/10.1039/c0dt00906g.

(28) Salazar, N.; Beinik, I.; Lauritsen, J. V. Single-Layer MoS_2 Formation by Sulfidation of Molybdenum Oxides in Different Oxidation States on Au(111). *Phys. Chem. Chem. Phys.* 2017, *19* (21), 14020–14029. https://doi.org/10.1039/c7cp00958e.

(29) Guimond, S.; Göbke, D.; Sturm, J. M.; Romanyshyn, Y.; Kuhlenbeck, H.; Cavalleri, M.; Freund, H. J. Well-Ordered Molybdenum Oxide Layers on Au(111): Preparation and Properties. *J. Phys. Chem. C* 2013, *117* (17), 8746–8757. https://doi.org/10.1021/jp3113792.

(30) Biener, M. M.; Friend, C. M. Heteroepitaxial Growth of Novel MoO_3 Nanostructures on Au(1 1 1). *Surf. Sci.* 2004, *559* (2–3), 173–179.

(31) Song, Z.; Cai, T.; Chang, Z.; Liu, G.; Rodriguez, J. A.; Hrbek, J. Molecular Level Study of the Formation and the Spread of MoO_3 on Au (111) by Scanning Tunneling Microscopy and X-Ray Photoelectron Spectroscopy. *J. Am. Chem. Soc.* 2003, *125* (26), 8059–8066. https://doi.org/10.1021/ja034862m.

(32) Biener, M. M.; Biener, J.; Schalek, R.; Friend, C. M. Growth of Nanocrystalline MoO_3 on Au(111) Studied by in Situ Scanning Tunneling Microscopy. *J. Chem. Phys.* 2004, *121* (23), 12010–12016. https://doi.org/10.1063/1.1808422.

(33) Uetsuka, H.; Onishi, H.; Ikeda, S.; Harada, Y.; Sakama, H.; Sakashita, Y. Atomic Force Microscope Observation of MoS_2 Particles Synthesized on Mica, MoS_2, and Graphite. *e-Journal Surf. Sci. Nanotechnol.* 2003, *1*, 80–83. https://doi.org/10.1380/ejssnt.2003.80.

(34) Mom, R. V.; Rost, M. J.; Frenken, J. W. M.; Groot, I. M. N. Tuning the Properties of Molybdenum Oxide on Al_2O_3/NiAl(110): Metal versus Oxide Deposition. *J. Phys. Chem. C* 2016, *120* (35), 19737–19743. https://doi.org/10.1021/acs.jpcc.6b06040.

(35) Haber, J.; Nowak, P.; Stoch, J. Molybdenum Oxide Monolayers at the Rutile (110) Surface Studied by Electrochemical and XPS Methods. *Bull. Polish Acad. Sci. Chem.* 1997, *45* (2), 139–149.

(36) Fester, J.; Bajdich, M.; Walton, A. S.; Sun, Z.; Plessow, P. N.; Vojvodic, A.; Lauritsen, J. V. Comparative Analysis of Cobalt Oxide Nanoisland Stability and Edge Structures on Three Related Noble Metal Surfaces: Au(111), Pt(111) and Ag(111). *Top. Catal.* 2017, *60* (6–7), 503–512. https://doi.org/10.1007/s11244-016-0708-6.

(37) De Santis, M.; Buchsbaum, A.; Varga, P.; Schmid, M. Growth of Ultrathin Cobalt Oxide Films on Pt(111). *Phys. Rev. B - Condens. Matter Mater. Phys.* 2011, *84* (12), 125430.

(38) Entani, S.; Kiguchi, M.; Saiki, K. Fabrication of Polar CoO(111) Thin Films on Pt(111). In *Surface Science*; 2004; Vol. 566–568, pp 165–169.

(39) Sebastian, I.; Heiler, M.; Meinel, K.; Neddermeyer, H. Growth of Epitaxial Layers of Co and CoO on Au(111). *Appl. Phys. A Mater. Sci. Process.* 1998, *66*, 525–528. https://doi.org/10.1007/s003390051195.

(40) Li, M.; Altman, E. I. Shape, Morphology, and Phase Transitions during Co Oxide Growth on Au(111). *J. Phys. Chem. C* 2014, *118* (24), 12706–12716. https://doi.org/10.1021/jp411375w.

(41) Li, M.; Altman, E. I. Cluster-Size Dependent Phase Transition of Co Oxides on Au(111). *Surf. Sci.* 2014, *619*, 6–10. https://doi.org/10.1016/j.susc.2013.09.029.

(42) Fester, J.; Sun, Z.; Rodríguez-Fernández, J.; Walton, A.; Lauritsen, J. V. Phase Transitions of Cobalt Oxide Bilayers on Au(111) and Pt(111): The Role of Edge Sites and Substrate Interactions. *J. Phys. Chem. B* 2018, *122* (2), 561–571. https://doi.org/10.1021/acs.jpcb.7b04944.

(43) Fester, J.; Walton, A.; Li, Z.; Lauritsen, J. V. Gold-Supported Two-Dimensional Cobalt Oxyhydroxide (CoOOH) and Multilayer Cobalt Oxide Islands. *Phys. Chem. Chem. Phys.* 2017, *19* (3), 2425–2433. https://doi.org/10.1039/c6cp07901f.

(44) Walton, A. S.; Fester, J.; Bajdich, M.; Arman, M. A.; Osiecki, J.; Knudsen, J.; Vojvodic, A.; Lauritsen, J. V. Interface Controlled Oxidation States in Layered Cobalt Oxide Nanoislands on Gold. *ACS Nano* 2015, *9* (3), 2445–2453. https://doi.org/10.1021/acsnano.5b00158.

(45) Chung, J. Bin; Chung, J. S. Desulfurization of H_2S Using Cobalt-Containing Sorbents at Low Temperatures. *Chem. Eng. Sci.* 2005, *60* (6), 1515–1523. https://doi.org/10.1016/j.ces.2004.11.002.

(46) Sanders, A. F. H.; De Jong, A. M.; De Beer, V. H. J.; Van Veen, J. A. R.; Niemantsverdriet, J. W. Formation of Cobalt-Molybdenum Sulfides in Hydrotreating Catalysts: A Surface Science Approach. *Appl. Surf. Sci.* 1999, *144–145*, 380–384. https://doi.org/10.1016/S0169-4332(98)00831-9.

(47) Coulier, L.; De Beer, V. H. J.; Van Veen, J. A. R.; Niemantsverdriet, J. W. On the Formation

of Cobalt-Molybdenum Sulfides in Silica-Supported Hydrotreating Model Catalysts. *Top. Catal.* 2000, *13* (1–2), 99–108. https://doi.org/10.1023/a:1009037006529.

(48) Leliveld, R. G.; Van Dillen, A. J.; Geus, J. W.; Koningsberger, D. C. A Mo-K Edge XAFS Study of the Metal Sulfide-Support Interaction in (Co)Mo Supported Alumina and Titania Catalysts. *J. Catal.* 1997, *165* (2), 184–196. https://doi.org/10.1006/jcat.1997.1480.

(49) Grønborg, S. S.; Salazar, N.; Bruix, A.; Rodríguez-Fernández, J.; Thomsen, S. D.; Hammer, B.; Lauritsen, J. V. Visualizing Hydrogen-Induced Reshaping and Edge Activation in MoS_2 and Co-Promoted MoS_2 Catalyst Clusters. *Nat. Commun.* 2018, *9* (1), 1–11.

(50) Herbschleb, C. T.; Van Der Tuijn, P. C.; Roobol, S. B.; Navarro, V.; Bakker, J. W.; Liu, Q.; Stoltz, D.; Cañas-Ventura, M. E.; Verdoes, G.; Van Spronsen, M. A.; Bergman, M.; Crama, L.; Taminiau, I.; Ofitserov, A.; Van Baarle, G. J. C.; Frenken, J. W. M. The ReactorSTM: Atomically Resolved Scanning Tunneling Microscopy under High-Pressure, High-Temperature Catalytic Reaction Conditions. *Rev. Sci. Instrum.* 2014, *85* (8), 83703. https://doi.org/10.1063/1.4891811.

(51) Rost, M. J.; van Baarle, G. J. C.; Katan, A. J.; van Spengen, W. M.; Schakel, P.; van Loo, W. A.; Oosterkamp, T. H.; Frenken, J. W. M. Video-Rate Scanning Probe Control Challenges: Setting the Stage for a Microscopy Revolution. *Asian J. Control* 2009, *11* (2), 110–129.

(52) Rost, M. J.; Crama, L.; Schakel, P.; Van Tol, E.; Van Velzen-Williams, G. B. E. M.; Overgauw, C. F.; Ter Horst, H.; Dekker, H.; Okhuijsen, B.; Seynen, M.; Vijftigschild, A.; Han, P.; Katan, A. J.; Schoots, K.; Schumm, R.; Van Loo, W.; Oosterkamp, T. H.; Frenken, J. W. M. Scanning Probe Microscopes Go Video Rate and Beyond. *Rev. Sci. Instrum.* 2005, *76* (5), 053710. https://doi.org/10.1063/1.1915288.

(53) Horcas, I.; Fernández, R.; Gómez-Rodríguez, J. M.; Colchero, J.; Gómez-Herrero, J.; Baro, A. M. WSXM: A Software for Scanning Probe Microscopy and a Tool for Nanotechnology. *Rev. Sci. Instrum.* 2007, *78* (1), 013705. https://doi.org/10.1063/1.2432410.

(54) Horcas, I.; Fernández, R.; Gómez-Rodríguez, J. M.; Colchero, J.; Gómez-Herrero, J.; Baro, A. M. WSXM: A Software for Scanning Probe Microscopy and a Tool for Nanotechnology. *Rev. Sci. Instrum.* 2007, *78* (1), 013705. https://doi.org/10.1063/1.2432410.

(55) Wagner, C. D. Sensitivity Factors for XPS Analysis of Surface Atoms. *J. Electron Spectros. Relat. Phenomena* 1983, *32* (2), 99–102. https://doi.org/10.1016/0368-2048(83)85087-7.

(56) Biesinger, M. C.; Payne, B. P.; Grosvenor, A. P.; Lau, L. W. M.; Gerson, A. R.; Smart, R. S. C. Resolving Surface Chemical States in XPS Analysis of First Row Transition Metals, Oxides and Hydroxides: Cr, Mn, Fe, Co and Ni. *Appl. Surf. Sci.* 2011, *257* (7), 2717–2730. https://doi.org/10.1016/j.apsusc.2010.10.051.

(57) van Haandel, L.; Smolentsev, G.; van Bokhoven, J. A.; Hensen, E. J. M.; Weber, T. Evidence of Octahedral Co–Mo–S Sites in Hydrodesulfurization Catalysts as Determined by Resonant Inelastic X-Ray Scattering and X-Ray Absorption Spectroscopy. *ACS Catal.* 2020, *10* (19), 10978–10988. https://doi.org/10.1021/acscatal.0c03062.

(58) Bremmer, G. M.; van Haandel, L.; Hensen, E. J. M.; Frenken, J. W. M.; Kooyman, P. J. The Effect of Oxidation and Resulfidation on (Ni/Co)MoS_2 Hydrodesulfurisation Catalysts. *Appl. Catal. B Environ.* 2019, *243*, 145–150. https://doi.org/10.1016/j.apcatb.2018.10.014.

(59) Deng, X.; Quek, S. Y.; Biener, M. M.; Biener, J.; Kang, D. H.; Schalek, R.; Kaxiras, E.; Friend, C. M. Selective Thermal Reduction of Single-Layer MoO_3 Nanostructures on Au(1 1 1). *Surf. Sci.* 2008, *602* (6), 1166–1174. https://doi.org/10.1016/j.susc.2008.01.014.

(60) Prabhu, M. K.; Boden, D.; Rost, M. J.; Meyer, J.; Groot, I. M. N. Structural Characterization of a Novel Two-Dimensional Material: Cobalt Sulfide Sheets on Au(111). *J. Phys. Chem. Lett.* 2020, *11* (21), 9038–9044. https://doi.org/10.1021/acs.jpclett.0c02268.

(61) Hebenstreit, E. L. D.; Hebenstreit, W.; Diebold, U. Adsorption of Sulfur on TiO_2(110) Studied with STM, LEED and XPS: Temperature-Dependent Change of Adsorption Site Combined with O-S Exchange. *Surf. Sci.* 2000, *461* (1–3), 87–97. https://doi.org/10.1016/S0039-6028(00)00538-0.

(62) Kibsgaard, J.; Morgenstern, K.; Lægsgaard, E.; Lauritsen, J. V.; Besenbacher, F. Restructuring of Cobalt Nanoparticles Induced by Formation and Diffusion of Monodisperse Metal-Sulfur Complexes. *Phys. Rev. Lett.* 2008, *100* (11), 116104. https://doi.org/10.1103/PhysRevLett.100.116104.

Chapter 4 - Supporting information

1. Moiré structure of Co oxide

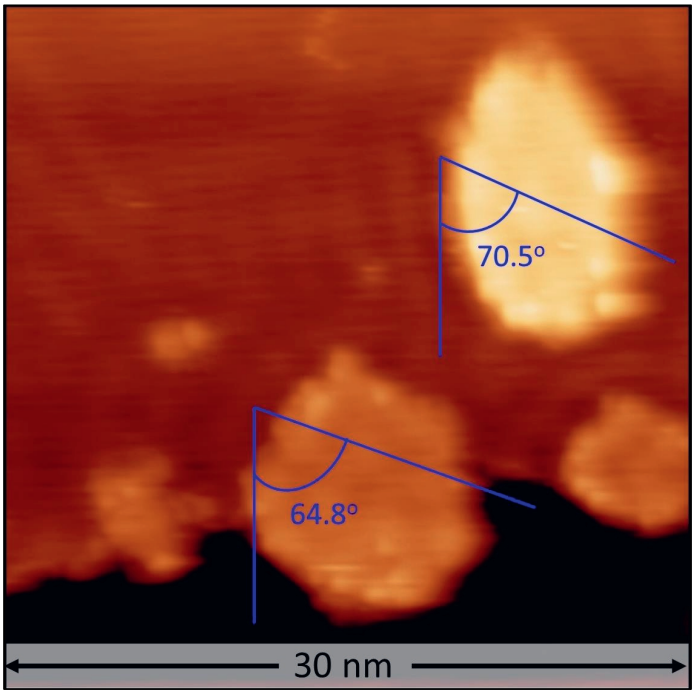

Figure S1: Angle measurement of the hexagonal moiré pattern on single- and double-layer Co-O type Co oxide slabs, tunneling current = 200 pA, sample voltage = -1.2 V. We measure a difference of ~6° in the direction of the moiré pattern of the higher slabs compared to the lower ones.

2. Synthesis of Mo oxide nanoparticles on Au(111)

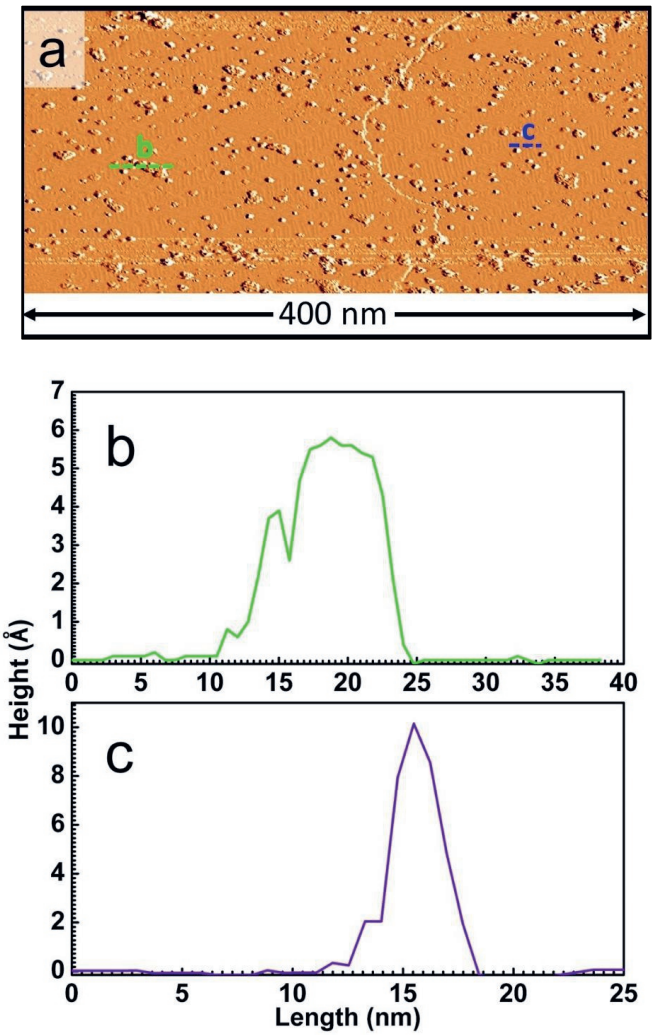

Figure S2: a) Large-scale STM image of Mo oxide nanoparticles on Au(111), sample voltage = -1.8 V, tunneling current = 200 pA. For clarity, the image is shown with a differential filter. The nanoparticles are grown by the direct deposition method described in the experimental section; b) measured height along line marked 'b' in Figure S2a; c) measured height along line marked 'c' in Figure S2a.

3. Measured STM heights of Co and Mo oxide nanoparticles supported on Au(111)

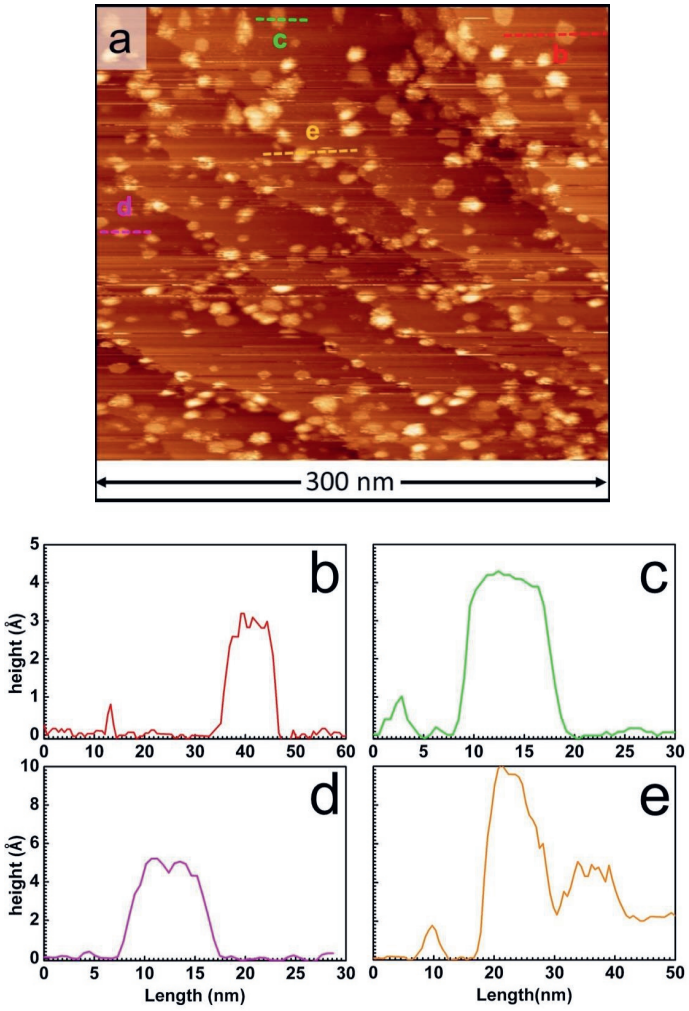

Figure S3: Mo and Co oxide nanoparticles on Au(111), sample voltage = -1.7 V, tunneling current = 150 pA; a) Large-scale STM image obtained at 300 K in UHV; b-d) Measured heights of Co oxide slabs along the dashed lines in Figure S3a with the respective colors, showing heights of 3 Å, 4 Å and 5 Å respectively; e) Measured height of an Mo oxide nanoparticle along the orange dashed line in Figure S3a showing a height of 10 Å.

4. Effect of increasing the duration of sulfidation and the temperature

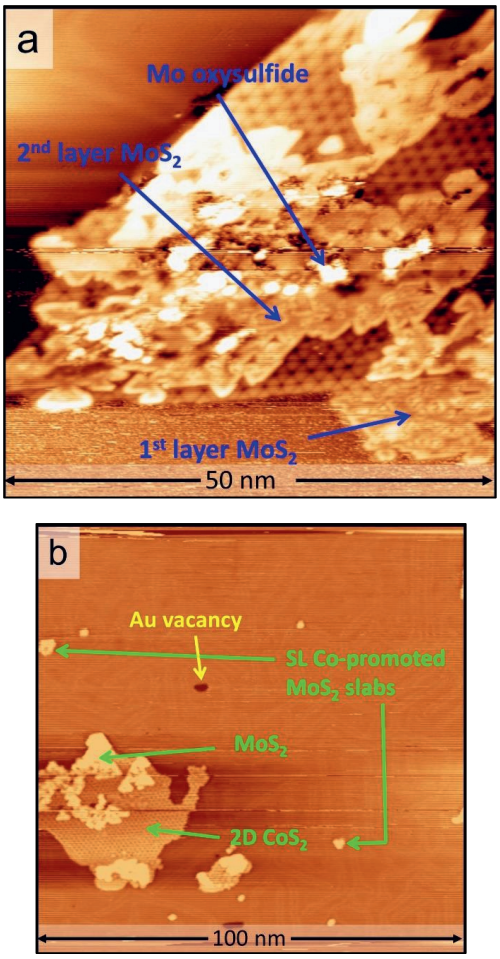

Figure S4: STM images after sulfidation of a mixture of Mo and Co oxides on Au(111), sample voltage = -1 V, tunneling current = 100 pA; a) at 650 K for 90 minutes, b) at 730 K for 25 minutes.

5. S 2p and O 1s XPS spectra

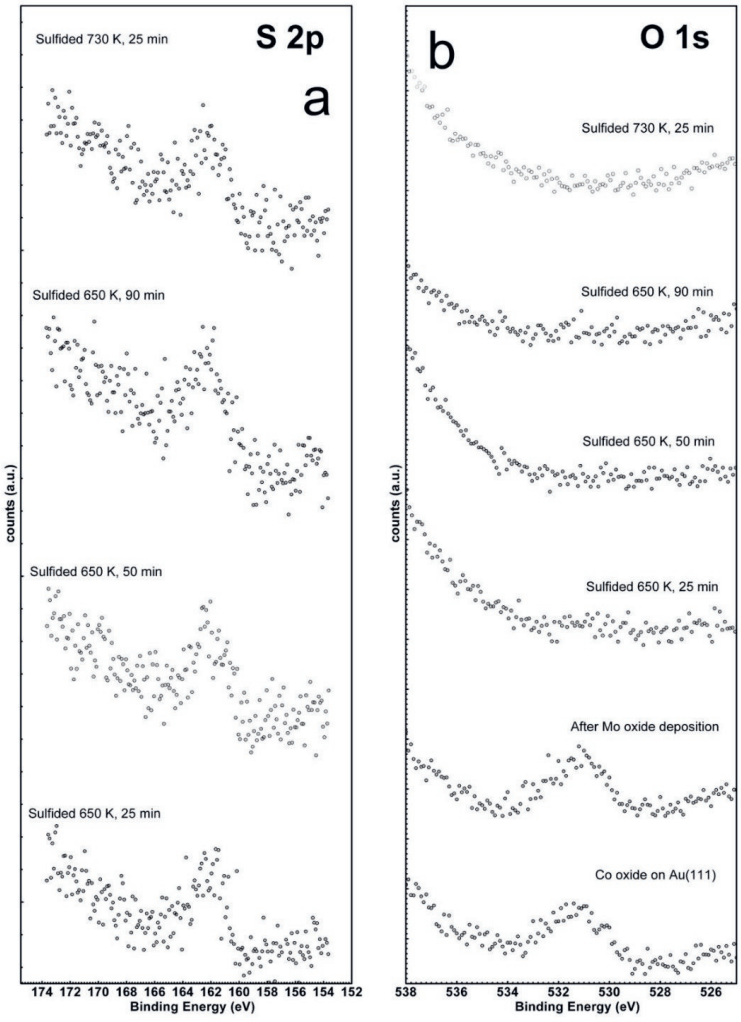

Figure S5:a,b) XPS spectra of S 2p and O 1s regions respectively at various stages of the oxide precursor synthesis and subsequent sulfidation.

6. Atomic model of the Co-promoted MoS_2 slab

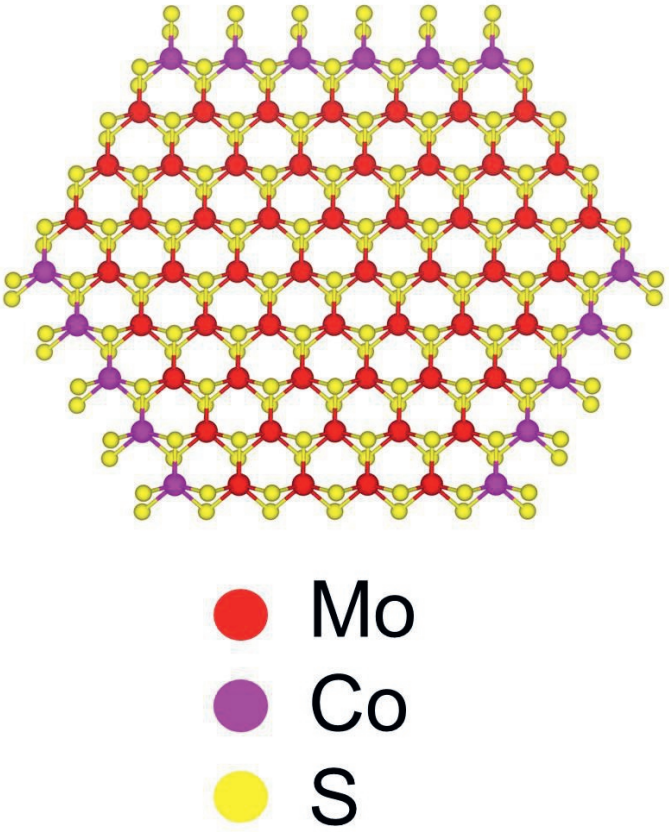

Figure S6: Atomic model of a Co-promoted MoS_2 slab.

7. Mixed Co and Mo oxide precursor heated in the absence of H_2S

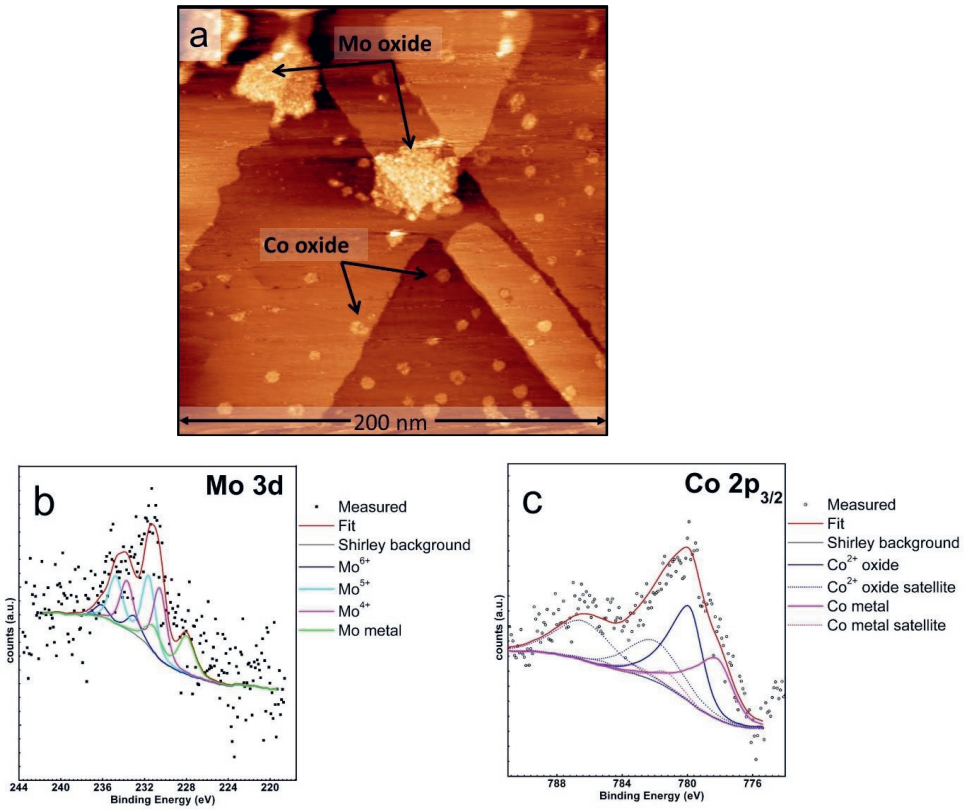

Figure S7: a) Large-scale STM image of a precursor containing Co oxide and Mo oxide slabs (as in Figure 2a) annealed at 650 K in a $5x10^{-7}$ mbar O_2 atmosphere, sample voltage = -1.5 V, tunneling current = 100 pA; b) Mo 3d XPS spectra of the sample in Figure S7a; c) Co $2p_{3/2}$ XPS spectra of the sample in Figure S7a.